Stochastic reservoir optimization using El Niño information: case study of Daule Peripa, Ecuador

Emiliano Gelati, Henrik Madsen and Dan Rosbjerg

ABSTRACT

Reservoir optimization requires the ability to produce inflow scenarios that are consistent with the available climatic information. We approach stochastic inflow modelling with a Markov-switching model where inflow anomalies are described by a mixture of autoregressive models with exogenous input, each corresponding to a hidden climate state. Climatic information is used as exogenous input and to condition state transitions. We apply the model to the inflow of the Daule Peripa reservoir in western Ecuador, where El Niño events cause anomalously heavy rainfall. El Niño–Southern Oscillation (ENSO) indices constitute the climatic input of the inflow model. The Daule Peripa reservoir serves a hydropower plant and a downstream water supply facility. Based on ENSO forecasts, which are available with 9 month lead time, monthly inflow scenarios are generated to perform stochastic optimization of reservoir releases with monthly time-steps. To account for inflow uncertainty, we generate multiple synthetic inflow time series and apply a multi-objective genetic algorithm to evaluate the objective functions. The results highlight the advantages of using a climate-driven stochastic model to produce inflow scenarios and forecasts for reservoir optimization, and show significant potential improvements with respect to the current reservoir management.

Key words | El Niño, genetic algorithms, inflow forecast, reservoir optimization

Emiliano Gelati (corresponding author)
Dan Rosbjerg
Department of Environmental Engineering,
Technical University of Denmark,
Miljøvej 113,
2800 Kongens Lyngby,
Denmark
E-mail: *emg@env.dtu.dk*

Henrik Madsen
DHI Water – Environment – Health,
Agern Allé 5,
2970 Hørsholm,
Denmark

ABBREVIATIONS

°	arc degrees
°C	Celsius degrees
ARX	autoregressive model with exogenous input
BS	dynamic programming benchmark solution
CO	combined operation
EM	expectation-maximization
ENSO	El Niño–Southern Oscillation
GA	genetic algorithm(s)
HO	historical operation
km	kilometers
LT	long-term operation
m	metres
MN	meganewtons
MW	megawatts
NSGA-II	non-dominated sorting genetic algorithm-II
PNWD	expected probability of not satisfying the downstream water demand
RMSD	expected root mean square hydropower deficit
s	seconds
SO	simulation-optimization
SSTA	sea surface temperature anomaly(ies)
ST	short-term operation
TNI	Trans-Niño Index

LIST OF SYMBOLS

$'$	transpose operator
a_m	observed inflow anomaly at month m

doi: 10.2166/nh.2011.009

$\mathbf{a}_{m_1:m_2}$	observed inflow anomaly time series from month m_1 to m_2
$\mathbf{b}_i$	auxiliary vector used in the EM algorithm to estimate the ARX parameters for climate state i
$c_m(i)$	ith ENSO-index at month m
$\mathbf{c}_m$	vector of ENSO-indices at month m
$\mathbf{C}_{m_1:m_2}$	observed ENSO-indices time series from month m_1 to m_2
$\widetilde{\mathbf{C}}_{m_1:m_2}$	forecasted ENSO-indices from month m_1 to m_2
$d_\alpha(m)$	sample standard deviation of the generic variable α for the calendar month corresponding to m
$E\{\ \}$	expectation operator
$e_\alpha(m)$	sample mean of the generic variable α for the calendar month corresponding to m
$f(a_m \mid s_m = i, a_{m-1}, \mathbf{c}_m, \theta)$	conditional probability density function of a_m, given $\mathbf{c}_m$, θ and that $s_m = i$.
g_t	average hydropower [MW] during time-step t
$g(r_t \mid h(\tau_{t-1}), q_t)$	function computing the hydropower generated by turbinating q_t during the time-step t given the initial water level $h(\tau_{t-1})$
G	maximum hydropower capacity (MW)
$\mathbf{G}^L_{m_1:m_2}$	set of L simulated hydropower time series from month m_1 to m_2
$\mathrm{h}(v(x))$	reservoir water level (m) as function of reservoir water volume at time x
$h_{\max}$	maximum reservoir water level (m)
$h_{\min}$	minimum reservoir water level (m)
h^m	water level at the end of monthly time-step m
$\mathbf{h}^{0:m}$	water level time series from the beginning of time-step 0 to the beginning of time-step m
$\mathbf{h}^{0:M}_*$	best water level time series from time-step 0 to M, according to the dynamic programming benchmark solution
$k(r_t)$	tailwater height (m) downstreams of the turbines as function of reservoir release
$l_m(i)$	raw value of the ith ENSO-index at month m
$o_i(j)$	jth objective value of policy i
$\mathbf{o}_i$	objective vector of policy i
p_{ij}	stationary component of the transition probability from climate state i to j
$\Pr\{\ \}$	probability operator
$q(x)$	reservoir inflow ($\mathrm{m^3\,s^{-1}}$) at time x
q_t	average reservoir inflow ($\mathrm{m^3\,s^{-1}}$) during time-step t
$\tilde{\mathbf{q}}_{m_1:m_2}$	synthetic inflow time series from month m_1 to m_2
$\widetilde{\mathbf{Q}}^L_{m_1:m_2}$	set of L synthetic inflow time series from month m_1 to m_2
$r(x)$	reservoir release ($\mathrm{m^3\,s^{-1}}$) at time x
r_t	average reservoir release ($\mathrm{m^3\,s^{-1}}$) during time-step t
r^{CO}_m	combined operation release during month m
r^{LT}_m	optimized long-term operation release during month m
r^{ST}_m	optimized short-term operation release during month m
$\mathbf{r}^*_{m:m+8}$	release time series from month m to $m+8$ that minimizes RMSD while guaranteeing that $U(\widetilde{\mathbf{Q}}^L_{m:m+8}, \mathbf{r}^*_{m:m+8}) \bar{U}$, given the forecast $\widetilde{\mathbf{Q}}^L_{m:m+8}$, according to the short-term operation
$R_{\max}$	maximum reservoir release ($\mathrm{m^3\,s^{-1}}$)
$R_{\min}$	minimum reservoir release ($\mathrm{m^3\,s^{-1}}$)
$\mathbf{R}^L_{m_1:m_2}$	set of L simulated release time series from month m_1 to m_2
s_m	climate state at month m
S	number of model-defined climate state
$u(r)$	dowstream water demand deficit Boolean function
$U(\widetilde{\mathbf{Q}}^L_{m_1:m_2}, \omega)$	expected probability of not satisfying the downstream water demand during a month as function of $\widetilde{\mathbf{Q}}^L_{m_1:m_2}$ and ω
$\bar{U}$	upper threshold for PNWD
$v(x)$	reservoir water volume ($\mathrm{m^3}$) at time x
$\mathbf{V}$	scale matrix used to compute climate state transition probabilities
$[w_p, w_\mu, w_{ARX}]$	set of auxiliary functions used in the EM algorithm
W	water supply facility demand ($\mathrm{m^3\,s^{-1}}$)
$\mathbf{X}_i$	auxiliary matrix used in the EM algorithm to estimate the ARX parameters for climate state i
$y_m(h^{m-1}, h^m)$	square hydropower deficit during the time-step m as function of h^{m-1} and h^m

$Y(\widetilde{\mathbf{Q}}^{L}_{m_1:m_2}, \omega)$ expected root mean square hydropower deficit (with respect to G) as function of $\widetilde{\mathbf{Q}}^{L}_{m_1:m_2}$ and ω

$\widehat{\alpha}^{(n)}$ estimate of the generic parameter α at the nth iteration of the EM algorithm

β turbine efficiency parameter

γ_i vector of ARX exogenous input parameters for climate state i

δ_i ARX intercept parameter for climate state i

ε turbine efficiency parameter

ζ_m Gaussian white noise process with zero mean and unit standard deviation

$\eta_i(m)$ upper water level corresponding to the ith release fraction for the calendar month corresponding to m

$\boldsymbol{\eta_i}$ vector of $\eta_i(m)$ for all calendar months (for $m = 1, \ldots, 12$)

$\boldsymbol{\theta}$ parameter set of the stochastic inflow model

$\widehat{\boldsymbol{\theta}}^{(n)}$ set of parameter estimates at the nth iteration of the EM algorithm

λ_i ARX autoregressive parameter for climate state i

$\boldsymbol{\mu_i}$ value of $\mathbf{c}_m$ maximizing the probability of shifting to climate state i

ν turbine efficiency parameter

ξ weight assigned to the optimized short-term release when computing the combined operation release

ρ_i ith release fraction

σ_i ARX standard deviation parameter for climate state i

τ_t end time (s) of time-step t

ϕ specific weight of water, 9.81×10^{-3} MNm^{-3}

χ_i ratio between η_{i+1} and η_i

ψ Lagrange multiplier used in the EM algorithm

ω reservoir operation policy

INTRODUCTION

According to the World Commission on Dams, most current reservoir operation policies are based on heuristic rules or subjective judgements of the operators. As a consequence, many large reservoir projects are not completely fulfilling the planning objectives (WCD 2000). Thus, the development of systematic and feasible approaches for optimizing reservoir management constitutes a priority. Moreover, enriching the optimization framework with additional information such as climatic forecasts would improve the efficiency of reservoir operation.

Several traditional methods to optimize single- and multi-reservoir systems, such as linear and dynamic programming, are reviewed by Yeh (1985) and Labadie (2004). However, these methods are affected by important drawbacks (Chen 2003). Linear programming requires the reservoir model to be linearized, e.g. by using piecewise linear functions (Loucks *et al.* 1981). The applicability of dynamic programming to multi-reservoir systems is hindered by the computational costs growing fast as the number of state variables increases. In many cases, these methods are therefore valid only for simplified reservoir systems.

The simulation-optimization (SO) approach, which combines simulation models with heuristic search procedures such as genetic algorithms (GA), overcomes some of the above limitations and facilitates implementation. Several studies have proved the efficacy of the SO approach: Oliveira & Loucks (1997) used GA to perform multi-objective optimization of complex reservoir systems with constraints on releases and hydropower production; Sharif & Wardlaw (2000) used GA to optimize a multi-reservoir system in the Brantas Basin in Indonesia; Chen (2003) applied a GA in combination with a simulation model to optimize the rule curves of a major reservoir system in Taiwan; and Ngo *et al.* (2007) used the shuffled complex evolution algorithm to optimize the Hoa Binh reservoir in Vietnam, focusing on the trade-off between flood control and hydropower generation.

The stochastic nature of inflow requires proper uncertainty handling to derive robust reservoir operation policies. Kelman *et al.* (1990) used stochastic dynamic programming to incorporate input uncertainty explicitly. Alternatively, uncertainty can be included implicitly by using sampling objective functions, which are evaluated on multiple synthetic input realizations (Tickle & Goulter 1994). Several water resources system optimizations were carried out by coupling GA with sampling objective functions, in order to reduce the amount of noise by taking the

mean of multiple noisy evaluations according to the Central Limit Theorem (Smalley & Minsker 2000; Gopalakrishnan *et al.* 2001; Kapelan *et al.* 2006; Wu *et al.* 2006).

In this study we consider the optimization of the Daule Peripa reservoir in Ecuador. We follow the SO approach and use the non-dominated sorting genetic algorithm-II (NSGA-II), which is a multi-objective GA (Deb *et al.* 2002), embedding sampling objective functions that account for the satisfaction of hydropower and downstream water demands. The Daule Peripa reservoir is located in western Ecuador where the occurrence of El Niño events, caused by positive sea-surface temperature anomalies (SSTA) in the equatorial Pacific Ocean, brings anomalously heavy rainfall (Vuille *et al.* 1999).

To account for the influence of El Niño–Southern Oscillation (ENSO), we applied the stochastic model by Gelati *et al.* (2010b) to generate synthetic inflow scenarios and forecasts. It is a mixture of autoregressive models with exogenous input (ARX), which use climatic variables as regressors. The ARX spells shift between each other according to a first-order Markov chain, where the transition probabilities depend on the current climatic information. The applied model is a Markov-switching model (Cappè *et al.* 2005) deriving from the work of Hamilton (1989), who modelled the gross domestic product with an autoregressive model conditioning the parameters on a hidden Markov chain that shifted between economic growth and recession phases. Such an approach was extended using a non-homogeneous Markov chain (i.e. with time-variant transition probabilities), which was previously applied in non-homogeneous hidden Markov models for precipitation downscaling studies (Hughes & Guttorp 1994; Hughes *et al.* 1999; Bellone *et al.* 2000; Robertson *et al.* 2004; Gelati *et al.* 2010a). Akintuğ & Rasmussen (2005) used Markov-switching models to generate annual streamflow time series, conditioning the runoff probability distribution on a hidden climate state following a Markov chain.

The modelling approach used in this study attempts to account for the climatic influence on inflow, and for the non-linearities in autocorrelation and between inflow and climatic variables. Synthetic inflow scenarios and forecasts, generated using ENSO information, are given as input to the reservoir simulation model to perform long- and short-term reservoir optimization.

This manuscript is part of the special issue of Hydrology Research entitled 'Regionalization of models for operational purposes in developing countries'. In this study, we address the problem of developing robust reservoir optimization methods that can handle climatic variability. The Daule Peripa case study in Ecuador represents a valid benchmark for testing the proposed methods, which exploit large-scale climatic information in a context of local data scarcity.

This paper has the following structure: we describe the Daule Peripa reservoir system, we define the reservoir simulation model and we illustrate the influence of ENSO on inflow; we outline the stochastic inflow model, describing parameter estimation and synthetic inflow generation; we describe the optimization algorithm, we formulate the sampling objective functions, we define the long-, short-term and combined operations and we derive a dynamic programming benchmark solution; we discuss the model-generated inflow scenarios and forecasts, as well as the optimization results; the achievements of the study are summarized; and in the appendix we describe the expectation-maximization algorithm, which is used for parameter estimation of the stochastic inflow model.

THE DAULE PERIPA RESERVOIR SYSTEM

The Daule Peripa reservoir is located in western Ecuador (2°S, 80°E), 5 km downstream of the confluence of the Daule and Peripa rivers (see Figure 1). The area of the drained catchment is approximately 4,200 km^2. Elevation is below 200 m, except for the north-eastern part where altitudes of up to 600 m are

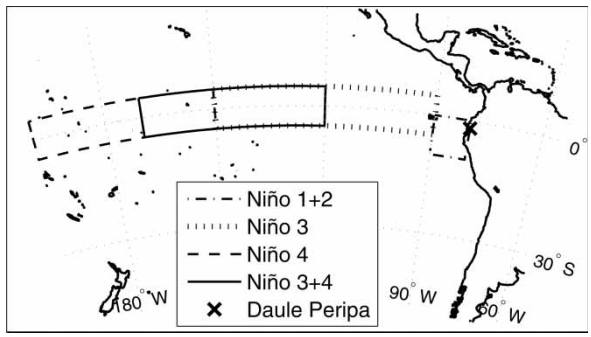

Figure 1 | Location of the Daule Peripa reservoir and areas of the Paciifc Ocean where the ENSO-related SST are measured (Gelati *et al.* 2010b).

reached. Average precipitation is higher in the north-eastern part (3,000 mm yr^{-1}) than in the rest of the catchment (2,200 mm yr^{-1}). No snowy precipitation is normally observed.

The reservoir construction was completed in 1987. The reservoir supplies a hydropower plant and an aggregate downstream water demand, which accounts for irrigation, urban water supply and environmental flows. Monthly inflow data are available from 1950 to 2008. The reservoir active storage volume is approximately 3.534 km^3, which corresponds to approximately 65% of average annual inflow volume. Average monthly inflow values are shown in Figure 2. Roughly 65% of annual inflow is concentrated in February, March and April. No systematic reservoir operation policy is known to the authors. However, reservoir water levels at the beginning of each month and monthly hydropower data are available from 2000 to 2008.

The reservoir simulation model

Due to the lack of data, we made the following assumptions: (i) all inflow is provided by the rivers Daule and Peripa; (ii) the reservoir storage is not affected by precipitation or evaporation occurring at its surface (indeed, these processes account for approximately 0.7% and 0.4% of average inflow); (iii) storage gains and losses due to filtration are negligible; and (iv) all released water flows through the turbines and is available to the water supply facility. Let G be the maximum hydropower capacity, W be the demand of the water supply facility, $R_{\min}$ and $R_{\max}$ be the minimum and maximum releases, and $h_{\min}$ and $h_{\max}$ be the minimum and maximum water levels. Their values are reported in Table 1.

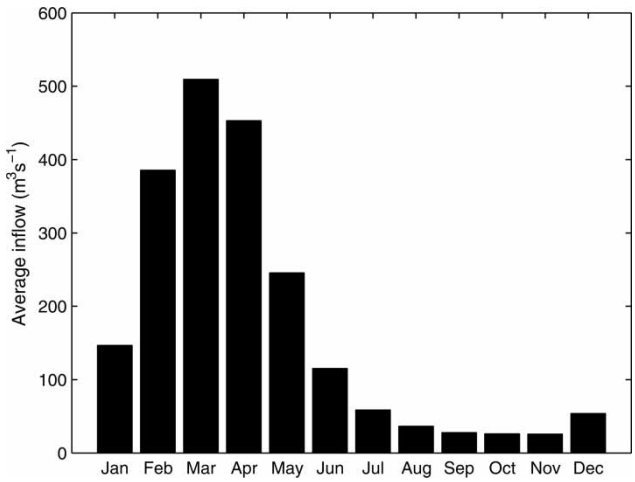

Figure 2 | Average monthly inflow computed from 1950–2008 data.

Table 1 | Summary of Daule Peripa reservoir characteristics

G (MW)	W ($m^3 s^{-1}$)	$R_{\min}$ ($m^3 s^{-1}$)	$R_{\max}$ ($m^3 s^{-1}$)	$h_{\min}$ (m)	$h_{\max}$ (m)
213	60	0	3,600	70	86

The reservoir system is simulated by subdividing the total time of simulation into T discrete time-steps of variable duration. Each time-step t is defined so that reservoir inflow and release can be assumed constant:

$$q(x) = q_t, \quad r(x) = r_t \quad \text{if } \tau_{t-1} \le x \le \tau_t \tag{1}$$

where τ_t is the end time of t; $q(x)$ and $r(x)$ are reservoir inflow and release at time x; and r_t and q_t are the average values of release and inflow during t.

According to the assumptions listed above, the reservoir mass balance during time-step t is:

$$v(x) = v(\tau_{t-1}) + (x - \tau_{t-1})(q_t - r_t) \tag{2}$$

where $v(x)$ is the reservoir water volume at time x. The level-volume relation was estimated as:

$$h(x) = h(v(x)) = 53.43 + \sqrt{2.225 \times 10^{-7} v(x) - 2.683 \times 10^2} \tag{3}$$

where $h(v(x))$ transforms the reservoir water volume into water level. Monthly reservoir releases were estimated from the observed water level and inflow time series by solving Equation (2) with monthly time-steps.

The average generated hydropower during time step t, g_t, is computed as:

$$g_t = g(r_t | h(\tau_{t-1}), q_t) = \frac{\phi \varepsilon r_t^{\beta}}{\tau_t - \tau_{t-1}} \int_{\tau_{t-1}}^{\tau_t} [h(x) - k(r_t)]^{\nu} \, dx \tag{4}$$

where ϕ is the specific weight of water (9.81×10^{-3} MN m^{-3}); ε, β and ν parameterize the turbine efficiency as a function of turbinated release and hydraulic head; and $k(r_t)$ denotes the tailwater height downstream of the turbines as function of r_t.

The turbine efficiency parameters were estimated via least squares regression using Equation (4), given the observed monthly release and hydropower time series. Figure 3 compares the estimated and observed monthly hydropower time series.

The influence of ENSO on reservoir inflow

The considered ENSO-indices are SSTA measured in several parts of the equatorial Pacific Ocean, namely Niño 1 + 2 (0–10°S, 90–80°W), Niño 3 (5°N–5°S, 150–90°W), Niño 3 + 4 (5°N–5°S, 170–120°W) and Niño 4 (5°N–5°S, 160°E–150°W) regions. The Trans-Niño Index (TNI), which is the difference between SSTA of the Niño 1 + 2 and Niño 4 regions (Trenberth & Stepaniak 2001), was also considered. Figure 1 shows the location of the Daule Peripa reservoir and the regions where the ENSO-related SSTA are measured. Monthly SST data were obtained for 1950–2008 from the NOAA Climate Prediction Center (Camp Springs, Maryland, USA; http://www.cpc.ncep.noaa.gov/data/indices/).

An overview of how ENSO indices correlate with inflow is presented in Figure 4 which shows the annual anomalies of inflow, Niño 1 + 2 SSTA and TNI. Annual anomalies were obtained by aggregating monthly data into annual time series, which were then standardized with respect to sample means and standard deviations. Among the considered ENSO indices, Niño 1 + 2 and TNI proved to be the best predictors for the Daule Peripa reservoir inflow (Gelati *et al.* 2010b). The annual time series indicate that ENSO-indices are more correlated with positive than with negative annual standardized inflow. El Niño conditions and westward SSTA gradients across the equatorial Pacific Ocean are well correlated with positive inflow anomalies, while La Niña does not have a significant impact on inflow (Gelati *et al.* 2010b). El Niño and La Niña phases of ENSO are associated with positive and negative SSTA in the equatorial Pacific Ocean (Trenberth 1997), respectively.

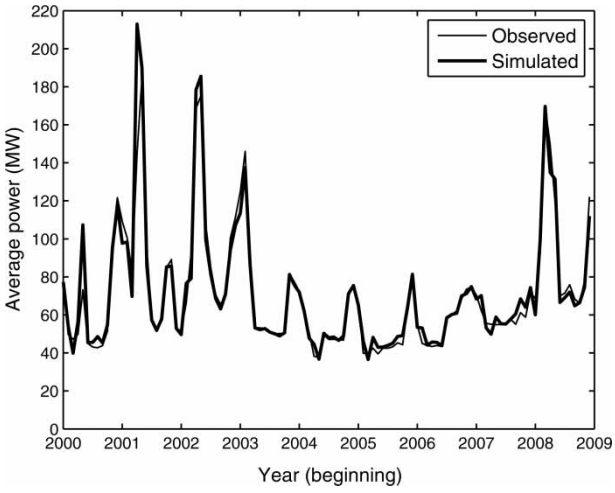

Figure 3 | Observed and estimated monthly hydropower time series.

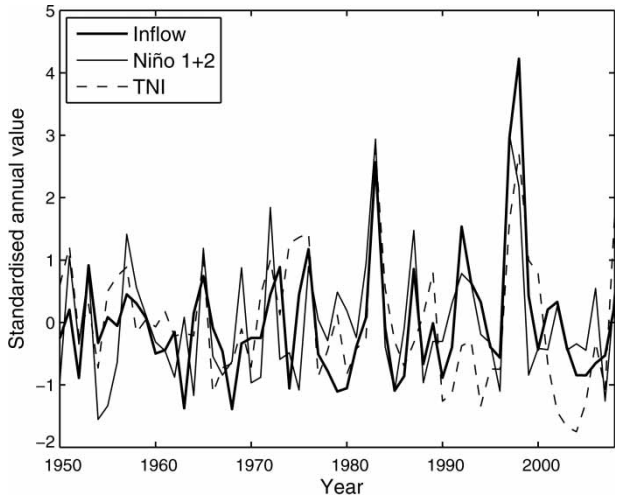

Figure 4 | Standardized annual time series of inflow, Niño 1 + 2, and TNI.

To apply the stochastic inflow model, ENSO-indices were de-seasonalized with respect to mean and standard deviation, while inflows were log-transformed before being de-seasonalized. Log-transformation was performed because of the significant positive skewness of raw inflow data, in order to be able to describe model noise with Gaussian distributions. The standardization methods are illustrated in Equations (5) and (6):

$$c_m(i) = \frac{l_m(i) - e_{l(i)}(m)}{d_{l(i)}(m)} \tag{5}$$

$$a_m = \frac{\log(q_m) - e_{\log(q)}(m)}{d_{\log(q)}(m)} \tag{6}$$

where $c_m(i)$ and a_m are the anomalies of the ith ENSO-index and inflow at month m, respectively; $l_m(i)$ and q_m are the raw values of the ith ENSO-index and inflow at month m,

respectively; and $e_z(m)$ and $d_z(m)$ are sample mean and standard deviation of the generic variable z for the calendar month corresponding to m, respectively.

A STOCHASTIC MODEL FOR RESERVOIR INFLOW CONDITIONED BY EL NIÑO INFORMATION

Model definition

The modelling approach presented by Gelati *et al.* (2010b) mimics ENSO-induced shifts between discrete inflow regimes and uses ENSO-indices as covariates to predict inflow. The model assumes inflow anomalies to be driven by a hidden climate state process. The climate state at month m is represented by the discrete stochastic variable s_m that can take on values $1, \ldots, S$. s_m follows a first-order Markov chain, where transition probabilities depend on the current ENSO-indices. Using the parameterization introduced by Hughes & Guttorp (1994) for non-homogeneous hidden Markov models, state transition probabilities are computed as:

$$\Pr\{s_m = j | s_{m-1} = i, \mathbf{c}_m, \boldsymbol{\theta}\} \propto p_{ij} \times \exp\left[-\frac{1}{2}(\mathbf{c}_m - \boldsymbol{\mu}_j)' \mathbf{V} (\mathbf{c}_m - \boldsymbol{\mu}_j)\right] \quad (7)$$

where $\mathbf{c}_m$ is the vector of ENSO-indices at month m; $\boldsymbol{\theta}$ is the parameter set; p_{ij} is the stationary component of the transition probability from state i to j; $\mathbf{V}$ is a scale matrix; $\boldsymbol{\mu}_i$ is the value of $\mathbf{c}_m$ that maximizes the probability of shifting to state i; and $'$ is the transpose operator. To guarantee parameter identifiability, p_{ij} is subject to the constraint $\sum_{j=1}^{S} p_{ij} = 1$ (for $i = 1, \ldots, S$). To reduce the number of free parameters, $\mathbf{V}$ is set equal to the inverse of the covariance matrix of $\mathbf{c}_m$ (Hughes & Guttorp 1994; Hughes *et al.* 1999; Bellone *et al.* 2000). State occurrence probabilities for the first time-step are calculated as:

$$\Pr\{s_1 = i | \mathbf{c}_1, \boldsymbol{\theta}\} \propto \exp\left[-\frac{1}{2}(\mathbf{c}_1 - \boldsymbol{\mu}_i)' \mathbf{V} (\mathbf{c}_1 - \boldsymbol{\mu}_i)\right] \quad (8)$$

where no stationary term is included, to limit parameter numerosity.

Inflow anomalies are modelled by an ARX spell, whose parameters are conditioned on the current climate state. Assuming the ARX spell noise to be a stationary Gaussian and independent process, the conditional probability density function of the inflow anomaly at month m reads:

$$f(a_m | s_m = i, a_{m-1}, \mathbf{c}_m, \boldsymbol{\theta}) = \frac{1}{\sigma_i \sqrt{2\pi}} \times \exp\left[-\frac{(a_m - \delta_i - \lambda_i a_{m-1} - \boldsymbol{\gamma}_i' \mathbf{c}_m)^2}{2\sigma_i^2}\right] \quad (9)$$

where a_m is the inflow anomaly at month m, defining a_0 to be zero, and δ_i, λ_i, $\boldsymbol{\gamma}_i$ and σ_i are the ARX parameters for state i.

The stochastic inflow model can be used for generating (i) inflow scenarios conditioned on records of ENSO-indices and (ii) inflow forecasts conditioned on ENSO forecasts and past observations. A thorough description of the inflow generation methods is available in Gelati *et al.* (2010b). For the purpose of model testing, we used observed ENSO data to generate synthetic inflow. In a real-life application, inflow would be forecasted using ENSO forecast data which are currently published with a 9 month lead time by the NOAA Climate Prediction Center.

Parameter estimation

The free parameter set is $\boldsymbol{\theta} = [p_{ij}, \boldsymbol{\mu}_i, \delta_i, \lambda_i, \boldsymbol{\gamma}_i, \sigma_i]$ (for $i = 1, \ldots, S$ and $j = 1, \ldots, S-1$). The model is calibrated via the expectation-maximization (EM) algorithm, which is an iterative maximum likelihood estimation method. It treats the hidden states as missing observations and requires initialization. The method was developed for hidden Markov models (Baum *et al.* 1970; Dempster *et al.* 1977) and later applied to non-homogeneous hidden Markov models by Hughes *et al.* (1999). The EM algorithm for the Markov-switching model used in this study is derived in the appendix.

OPTIMIZATION TECHNIQUES

To optimize the Daule Peripa reservoir, we coupled the reservoir simulation model with a heuristic search method. The applied SO approach consists of the following

procedure: (i) sets of reservoir operation decision variables, referred to as policies, are randomly generated; (ii) for each policy, the objective functions are evaluated by the reservoir simulation model; (iii) according to such evaluations, the optimization algorithm generates new policies; and (iv) steps (ii) and (iii) are iterated until a termination criterion is satisfied. In this section, we outline the optimization framework by formulating the objective functions; describe the optimization algorithm; and define the long- and short-term operation policies to be optimized as well as their combination. Finally, we derive a dynamic programming solution to benchmark the optimized policies.

Objective functions

The main purposes of the Daule Peripa reservoir are hydropower production and water supply. Although the turbinated release is available to the downstream water supply facility, water uses are conflicting. Maximizing hydropower production requires high hydraulic heads at the turbines, to maximize the specific energy yield of the turbinated flow. This may result in reservoir releases not satisfying the downstream water demand, when it is more convenient to refill the reservoir than to turbinate.

The downstream water demand satisfaction might be treated as a constraint, thus leading to a constrained single-objective optimization problem. We believe that treating the downstream water demand satisfaction as an additional objective may help the decision-making process, since a multi-objective optimization approach reveals the trade-off between objectives.

Objective functions are evaluated by simulating the reservoir with a number of synthetic inflow time series and taking the mean of the objective values obtained for each time series. Such objective functions are referred to as sampling objective functions. Sampling objective functions allow a more thorough exploration of the objective space, facilitating the reservoir operator in choosing the best compromising policy. As sampling objective functions help account for input uncertainty, they are likely to yield robust operation policies.

The number of synthetic inflow time series used to compute the sampling objective functions is decided according to the following criteria: (i) if simulations are repeated on several sets of synthetic inflow time series, the sampling objective functions of a policy must take similar values (stability criterion) and (ii) the computational cost of evaluating the sampling objective functions must be acceptable (feasibility criterion). Increasing the number of time series favours stability but penalizes feasibility; a compromise is therefore needed.

Let $\widetilde{\mathbf{Q}}^{L}_{m_1:m_2} = [\widetilde{\mathbf{q}}^{(1)}_{m_1:m_2}, \ldots, \widetilde{\mathbf{q}}^{(L)}_{m_1:m_2}]$ be a set of L synthetic inflow time series from month m_1 to m_2; let ω be a generic policy; and let $\mathbf{R}^{L}_{m_1:m_2} = [\mathbf{r}^{(1)}_{m_1:m_2}, \ldots, \mathbf{r}^{(L)}_{m_1:m_2}]$ and $\mathbf{G}^{L}_{m_1:m_2} = [\mathbf{g}^{(1)}_{m_1:m_2}, \ldots, \mathbf{g}^{(L)}_{m_1:m_2}]$ be the sets of corresponding release and hydropower time series, obtained by simulating the reservoir implementing ω given $\widetilde{\mathbf{Q}}^{L}_{m_1:m_2}$. The reservoir is simulated with time-steps that do not exceed 1 month duration. During simulation time-steps, inflow and release are assumed to be constant and inflow is available at a monthly timescale. To compute the objective functions, simulated release and hydropower are aggregated into monthly values.

The sampling objective function estimating the expected probability of not satisfying the downstream water demand W during a month (PNWD) is:

$$U(\widetilde{\mathbf{Q}}^{L}_{m_1:m_2}, \omega) = \frac{1}{L(1+m_2-m_1)} \sum_{l=1}^{L} \sum_{m=m_1}^{m_2} u(r^{(l)}_m) \tag{10}$$

where

$$u(r) = \begin{cases} 0 & \text{if } r \geq W \\ 1 & \text{if } r < W \end{cases} \tag{11}$$

The sampling objective function estimating the expected root mean square hydropower deficit (RMSD), assuming the maximum hydropower capacity G to be the demand, is:

$$Y(\widetilde{\mathbf{Q}}^{L}_{m_1:m_2}, \omega) = \sqrt{\frac{1}{L(1+m_2-m_1)} \sum_{l=1}^{L} \sum_{m=m_1}^{m_2} \left(G - g^{(l)}_m\right)^2} \tag{12}$$

Optimization algorithm

Multi-objective optimization can be approached with either aggregation or Pareto domination methods. Aggregation methods aggregate the objective functions into a single

scalar value, e.g., by using weights. In Pareto domination methods, policies are evaluated using the concept of Pareto dominance (Burke & Silva 2006). In a set, a policy is Pareto-dominated if there is at least another policy performing not worse in all objectives and better in at least one objective.

NSGA-II (Deb *et al.* 2002) was chosen as the optimization algorithm for this application. It is a multi-objective genetic algorithm that uses Pareto dominance to rank policies. NSGA-II can be briefly summarized as follows: (i) an initial set of policies is randomly generated; (ii) objective functions are evaluated for each member of the initial set; (iii) a new set is generated by applying the genetic operators (selection, crossover and mutation) to the initial set; (iv) objective functions are evaluated for each member of the new set; (v) initial and new sets are aggregated into a joint set; (vi) the fast non-dominated sorting algorithm ranks the members of the joint set according to Pareto dominance; (vii) the crowding distance operator selects a new initial set; (viii) steps from (ii) to (vii) are iterated until a termination criterion is satisfied. The genetic operators, the fast non-dominated sorting algorithm, and the crowding distance operator are described in detail by Deb *et al.* (2002).

Long-term operation

We decided to define long-term operation (LT) with a set of rule curves that determine the release as function of storage and calendar month. Alternatively, rule curves may guide releases as functions of storage and inflow. The ith rule curve $\boldsymbol{\eta}_i = [\eta_i(1), \ldots, \eta_i(12)]$ reads, for each month, the upper water level corresponding to the release fraction ρ_i. Rule curves and release fractions are defined so that $\rho_i < \rho_{i-1}$ and $\eta_i(z) < \eta_{i-1}(z)$ for $z = 1, \ldots, 12$.

We assume that N rule curves have to be specified to define LT. To fulfill the water level constraints (Table 1), we need to introduce two additional rule curves and release fractions: $\rho_0 = 1$ and $\rho_{N+1} = 0$, and $\eta_0(z) = h_{\max}$ and $\eta_{N+1}(z) = h_{\min}$ for $z = 1, \ldots, 12$. To limit the number of decision variables to be optimized, $\boldsymbol{\eta}_1$ is defined as a set of independent levels while the remaining rule curves are defined as:

$$\boldsymbol{\eta}_i = h_{\min} + \chi_{i-1}(\boldsymbol{\eta}_{i-1} - h_{\min}) \quad \text{for } i = 2, \ldots, N. \tag{13}$$

Thus LT is defined by $11 + N$ independent decision variables $\boldsymbol{\eta}_1, \chi_1, \ldots, \chi_{N-1}$ which have to be optimized fulfilling the constraints:

$$h_{\min} < \eta_1(z) < h_{\max} \quad \text{for } z = 1, \ldots, 12 \tag{14}$$

$$0 < \chi_i < 1 \quad \text{for } i = 1, \ldots, N-1. \tag{15}$$

To evaluate LT, the reservoir is simulated using synthetic inflow scenarios $\widetilde{\mathbf{Q}}^L_{1:M}$ generated by conditioning on the observed ENSO-indices $\mathbf{C}_{1:M}$. During time-step t falling in month m (corresponding to the zth calendar month), given that $\eta_{i+1}(z) < h(x) \leq \eta_i(z)$ for $\tau_{t-1} \leq x \leq \tau_t$, the release is computed as:

$$r_t = \rho_{i-1} g^{-1}(G | h(\tau_{t-1}), \tilde{q}_m) \tag{16}$$

where the function $g^{-1}(G|h(\tau_t), \tilde{q}_m)$ is the inverse of Equation (4) and computes the release to be turbinated during t to generate hydropower at the maximum capacity G, given the initial water level $h(\tau_{t-1})$ and the synthetic inflow $\tilde{q}_m$. The time-step length is variable, cannot exceed 1 month duration, and is determined so that inflow and release can be assumed constant.

Short-term operation

The short-term operation (ST) is optimized at the beginning of each monthly time-step. It exploits past observations and current ENSO forecasts, which are available with a 9 month lead time, to decide the release during the upcoming month. At the beginning of the monthly time-step m, the reservoir releases $\mathbf{r}_{m:m+8} = [r_m, \ldots, r_{m+8}]$ are the variables to be optimized. The reservoir is simulated with a set of inflow forecast time series $\widetilde{\mathbf{Q}}^L_{m:m+8}$, which is generated by conditioning of past observations ($\mathbf{a}_{0:m-1}$ and $\mathbf{C}_{1:m-1}$) and ENSO forecasts $\widetilde{\mathbf{C}}_{m:m+8}$. As the optimization returns a set of non-dominated policies, the best series of releases $\mathbf{r}^*_{m:m+8}$ must be chosen according to a preference criterion.

We assumed that the operator decides an upper threshold $\bar{U}$ for PNWD, setting the maximum acceptable probability of downstream water deficit. Thus $\mathbf{r}^*_{m:m+8}$ is chosen as the series of releases minimizing RMSD while

guaranteeing that

$$U(\tilde{\mathbf{Q}}^{L}_{m:m+8}, \mathbf{r}^{*}_{m:m+8}) \leq \bar{U}$$

During the monthly time-step m, r^{*}_{m} is implemented, the inflow q_m and the ENSO anomalies $\mathbf{c}_m$ are observed and the water level is updated. The optimization procedure is repeated for time-step $m+1$, and so on. By optimizing 9 monthly releases and implementing only the first release at each time-step, over- or under-exploitation of the water resource can be partly corrected due to the update of reservoir level, inflow and climatic data.

Combined operation

To exploit the short-term climatic information brought by the ENSO forecasts while preserving the long-term objectives, we defined an operation scheme that combines the results of the short- and long-term optimizations. Thus the combined operation (CO) defines the release as a weighted average of the optimized short- and long-term operation releases:

$$r^{CO}_{m} = \xi r^{ST}_{m} + (1-\xi) r^{LT}_{m} \tag{17}$$

where r^{CO}_{m}, r^{ST}_{m} and r^{LT}_{m} are the releases of the combined, short- and long-term operations and $0 \leq \xi \leq 1$ is the weight assigned to the optimized short-term operation. Thus CO allows a compromise to be made between the solution optimized for the forecast horizon and the long-term objectives (Todini 1999).

Dynamic programming benchmark solution

To benchmark the improvement brought by the optimized operation policies with respect to the current management, we applied the dynamic programming (DP) algorithm (Bellman 1957; Bertsekas 2000). Given a discrete set of possible water levels, assuming perfect knowledge of the inflow time series, the DP algorithm can be applied to find the monthly time series of water levels minimizing RMSD and meeting the downstream water demand at all time-steps. Let us denote the water level at the end of the monthly time-step m by h^m. We assume that h^m can take on a discrete set of water levels X, so that if $h \in X$ then $h_{\min} \leq h \leq h_{\max}$. Given the inflow q_m, release and hydropower during m are functions of h^{m-1} and h^m:

$$r_m = r_m(h^{m-1}, h^m) \tag{18}$$

$$g_m = g_m(h^{m-1}, h^m) \tag{19}$$

where r_m and g_m are, respectively, release and average hydropower during m. To ensure the satisfaction of the downstream water demand, the square hydropower deficit for m is defined as

$$y_m(h^{m-1}, h^m) = \begin{cases} (G - g_m)^2 & \text{if } W \leq r_m \leq R_{\max} \\ \infty & \text{otherwise} \end{cases} \tag{20}$$

Denoting the water level time series $[h^0, \ldots, h^m]$ by $\mathbf{h}^{0:m}$, RMSD for the time-steps up to m is evaluated as:

$$Y(\mathbf{h}^{0:m}) = \sqrt{\frac{1}{m}\sum_{i=1}^{m} y_i(h^{i-1}, h^i)} \tag{21}$$

The DP algorithm therefore finds $\mathbf{h}^{0:M}_{*} = [h^0_{*}, \ldots, h^M_{*}]$, solving the minimization problem:

$$\mathbf{h}^{0:M}_{*} = \arg\min_{\mathbf{h}^{0:M}} \left\{ Y\left(\mathbf{h}^{0:M}\right) \right\} \tag{22}$$

where M is the last monthly time-step. In this application, h^0_{*} and h^M_{*} are constrained to equal the corresponding observed values.

RESULTS AND DISCUSSION

In this section we first give an overview of the inflow scenarios and forecasts generated by the stochastic inflow model. We then illustrate the outcomes of optimizing LT during 1950–1999, for which no information about historical operation (HO) is available. Finally, for the period 2000–2008 we compare LT, ST, CO, HO and the dynamic programming

benchmark solution (BS). The number of synthetic inflow time series used for reservoir simulation was set to 100, as it constituted the best compromise between computational feasibility and the stability of sampling objective functions.

Generated inflow scenarios and forecasts

A 2-state model set-up using Niño 1 + 2 SSTA and TNI as ENSO-indices was calibrated using 1950–1999 monthly time series. Figure 5(a) illustrates the reproduction of observed mean annual inflow by model-generated inflow scenarios. Simulated annual inflow is obtained by aggregating simulated monthly values. Observed annual inflows are well approximated by the expected values estimated from the generated scenarios. Exceptions are the lowest values and those of 1983 and 1997, which are overestimated. However, most observed values are included by the 10% and 90% sampling quantiles of the generated scenarios, thus indicating a general good reproduction of annual inflow.

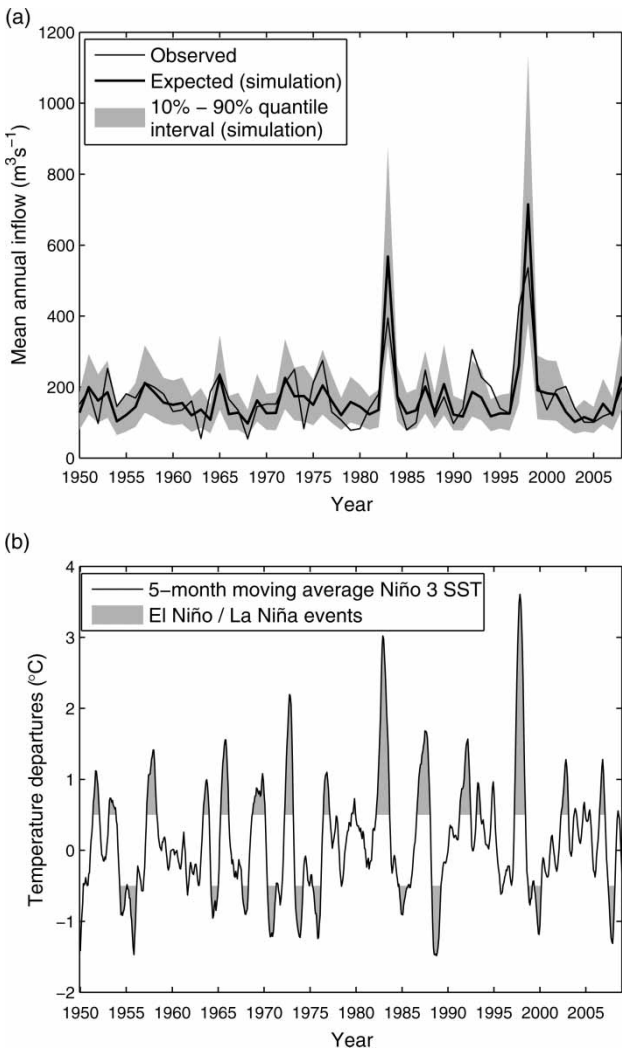

Figure 5 | Time series of (a) observed and model-generated mean annual inflow and (b) 5 month moving average of Niño 3 SST departures from monthly mean values, where the shaded areas indicate El Niño and La Niña events.

The El Niño and La Niña events that occurred in the period 1950–2008 are reported in Figure 5(b), according to the definition by Trenberth (1997). A comparison of Figures 5(a) and (b) reveals that most observed annual inflow peaks correspond to El Niño events. In most cases, expected synthetic annual inflow also has a peak, reasonably approximating the observations (1953–1954, 1957–1958, 1965–1968, 1972–1973, 1976–1977 and 1987 events). In few cases synthetic values significantly underestimate the observations (1992 and 2002 events), while overestimation occurs for the two major El Niño events (1982–1983 and 1997–1998). In contrast, La Niña events do not appear to be significantly correlated with annual inflow. Annual inflow gives an idea of how the stochastic model can predict inflow regime fluctuations. Details about the reproduction of other inflow statistics can be found in Gelati *et al.* (2010b).

Expected values of monthly inflow forecasts are compared to observations in Figure 6. Although low values tend to be overestimated, inflow is reasonably forecasted. The accuracy slightly diminishes when increasing the forecast lead time: the Nash–Sutcliffe coefficient (Nash & Sutcliffe 1970) scored 0.63 and 0.61 for 1 and 9 month lead times, respectively.

Optimized long-term operation (1950–1999)

LT was optimized using synthetic inflow scenarios that were generated using the 1950–1999 ENSO-indices record. To choose the best set of release fractions, a large number of optimization trials were performed. This search aimed at obtaining optimized rule curves that had a sufficient level of resolution without overlapping. The chosen release fractions are 0.4, 0.3, 0.25, 0.2, 0.15 and 0.125, thus defining an optimization problem with 17 decision variables.

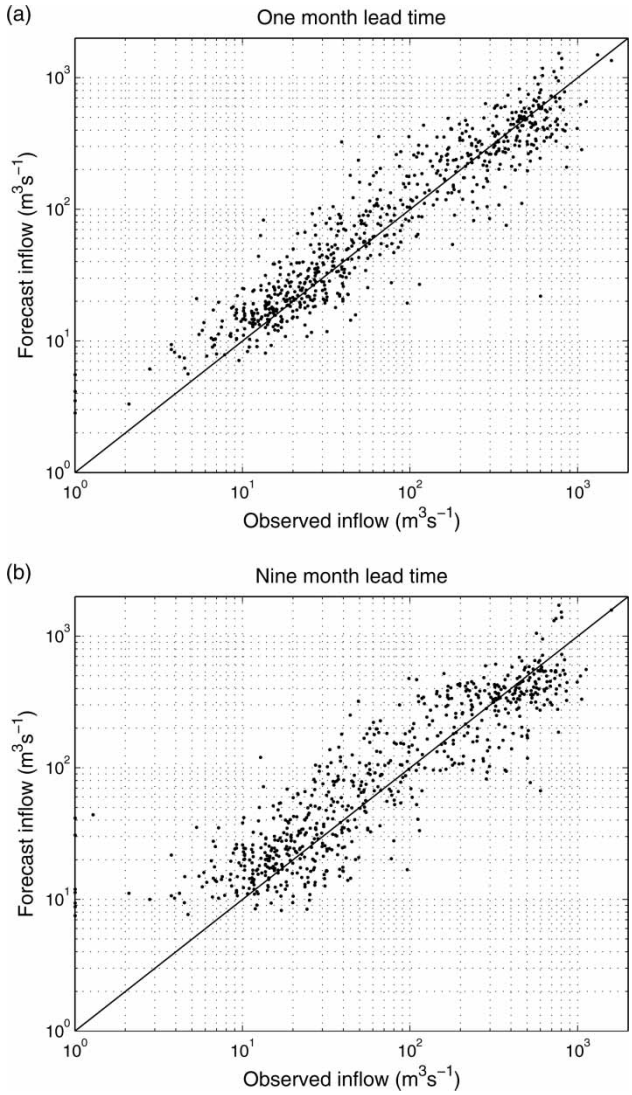

Figure 6 | Observed monthly inflow versus expected values of inflow forecasts for (a) 1 and (b) 9 month lead times.

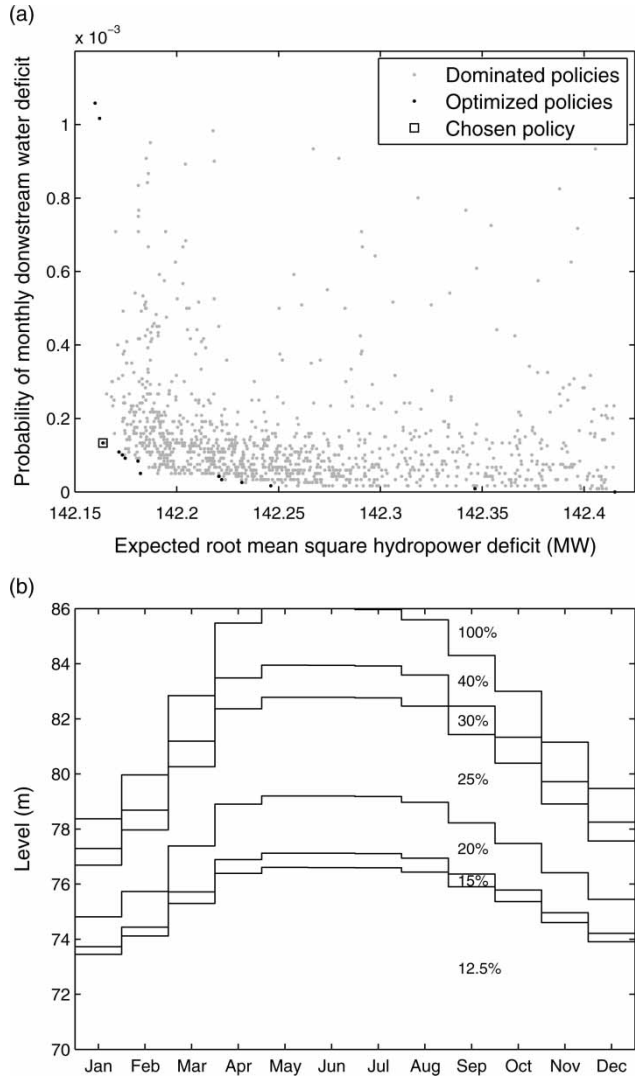

Figure 7 | Optimized long-term operation policies: (a) objectives space representation of the non-dominated policies and (b) rule curves defining the chosen policy.

Figure 7(a) shows the found non-dominated policies in the objective space. Of the non-dominated policies, we assumed that the operator would adopt the policy minimizing RMSD while yielding PNWD smaller than 10^{-3}. The rule curves defining the chosen policy (LT) are plotted in Figure 7(b).

The February–April average inflow is comparable to the reservoir active storage volume (3.534×10^9 m^3), corresponding to 65% of the average annual inflow. Applying LT during an average hydrologic year, the reservoir water level typically reaches its maximum between April and June. Between May and July LT sets higher level requirements for releasing water, in order not to empty the reservoir before the following dry months. Level requirements for releasing water decrease between October and March, so that the reservoir can be filled during the wet months without any spill. During such months, high water levels are less likely and, if occurring, lead to anomalously large releases.

Figure 8 reports the water level, release and hydropower time series obtained by simulating LT with observed and synthetic inflow. When LT is simulated using inflow observations, the reservoir is never completely emptied and no

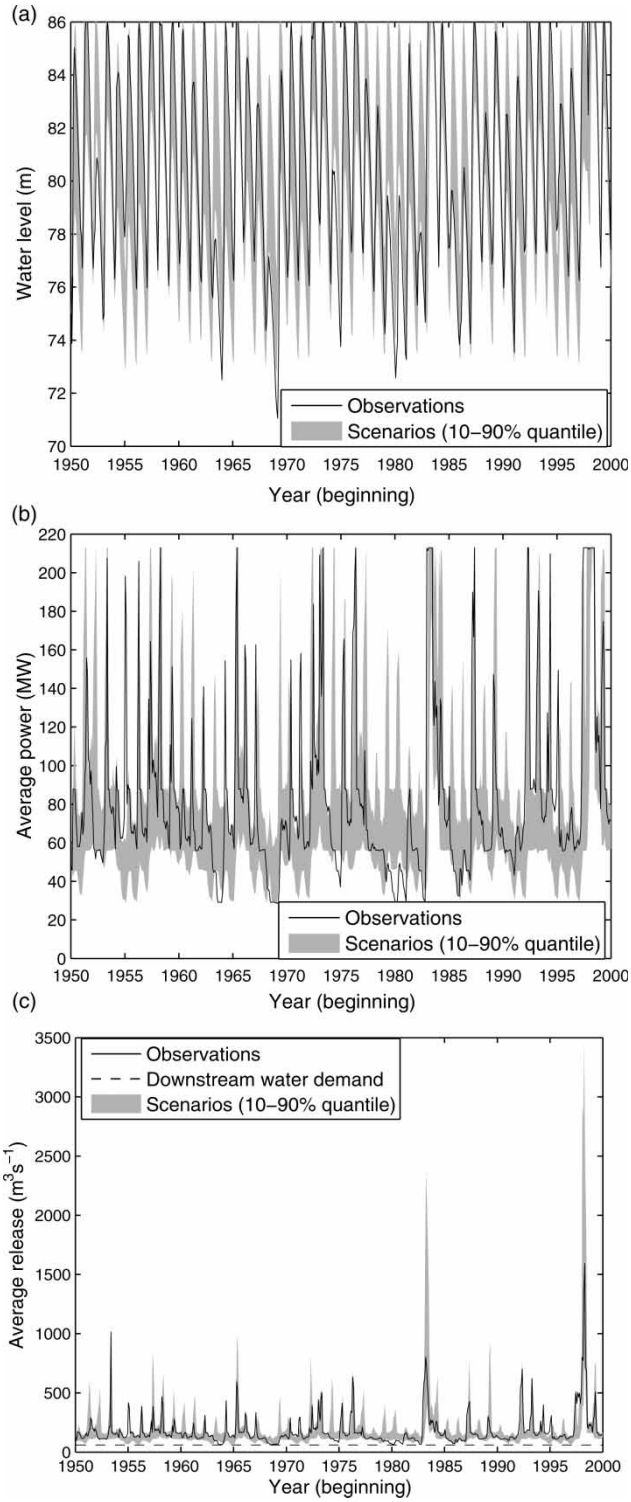

Figure 8 | Time series obtained by simulating the chosen long-term policy on inflow observations and scenarios (1950–1999): (a) reservoir water level at the beginning of each month, (b) average monthly hydropower and (c) average monthly reservoir release.

downstream water deficit occurs. Water level fluctuations obtained with observed inflow are generally contained in the 10–90% quantile band obtained with synthetic inflow, except for lowest minima. Similarly, hydropower and release values simulated with observed inflow are reasonably predicted by the simulation with synthetic inflow scenarios. However, the lowest minima are not included by the 10–90% quantile band. The less accurate reproduction of minima is due to the limited ability of the stochastic inflow model to predict anomalously low inflow. In contrast, at the occurrence of El Niño events when inflow is anomalously large, the behaviour of the reservoir is satisfactorily predicted by simulating LT with synthetic inflow.

Optimized short-term and combined operations (2000–2008)

For the period 2000–2008, information about HO is available. HO was evaluated using the reservoir simulation model. We compare the performances of ST, CO, LT, HO and BS during 2000–2008. ST was optimized during 2000–2008 by setting $\bar{U} = 10^{-3}$. LT was optimized during 1950–1999 and then applied to the period 2000–2008. The optimal value of the weight ξ, which defines CO given LT and ST, was found to be 0.78 during 1950–1999; such a value was then used to evaluate CO for the period 2000–2008.

All operations were simulated using the observed 2000–2008 monthly inflow time series (Figure 9).

Table 2 reports performance indicators of the tested reservoir operations: all operations always meet the downstream water demand W while CO performs better than ST, LT and HO if considering RMSD and average hydropower production. Also looking at spills, which occur when the release exceeds the flow that needs to be turbinated to produce the maximum hydropower capacity, CO performs best.

The chosen indicators suggest that CO, ST and LT may improve the Daule Peripa reservoir management with respect to HO, and that CO is the best alternative. Given a set of water level discretizations and assuming perfect knowledge of inflow, BS minimizes RMSD while constraining PNWD to be zero. Thus BS estimates a boundary for operational improvement in terms of RMSD, while

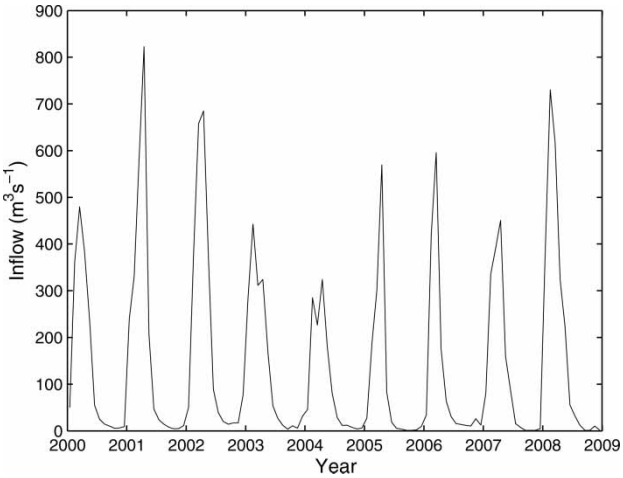

Figure 9 | Observed monthly inflow time series for the period 2000–2008.

Table 2 | Reservoir operation performance indicators evaluated for: historical operation (HO); long-term operation optimized during 1950–1999 (LT); short-term operation (ST); combined operation (CO); and dynamic programming benchmark solution (BS)

Operation	RMSD (MW)	PNWD (–)	Average power (MW)	Average spill ($m^3 s^{-1}$)
HO	147.0	0	70.64	2.34
LT	144.8	0	71.36	1.48
ST	143.7	0	71.80	0
CO	143.2	0	72.80	0
BS	139.8	0	74.68	0

satisfying the downstream water demand. Because of water level discretization, BS provides an estimate and not the real boundary. However, the estimate is reliable, since a high water level resolution (0.1 m) is used. BS estimates the maximum possible RMSD reduction to be 4.9% of the value computed for HO. LT, ST and CO yield 1.5, 2.2 and 2.6% RMSD reductions, respectively. Thus, CO yields roughly half of the estimated possible improvement. Moreover, CO increases the average hydopower production by 3.1% compared to HO. Average hydopower is increased by 5.7, 1.6 and 1.0% when applying BS, ST and LT, respectively.

The time series of simulated water level, hydropower, release and release fraction are illustrated in Figure 10. Release fraction is the ratio between release and the flow that needs to be turbinated to produce the maximum hydropower capacity, which is estimated by inverting Equation (4). According to BS water levels (Figure 10(a)), it is optimal to fill the reservoir by the end of each wet season (between April and June) and to lower the water level until December–January to leave available storage volume for the following wet season.

Such behaviour is reasonably mimicked by CO until the end of the 2003 wet season. Due to misprediction of the 2004 anomalously low inflow (Figure 9), the CO water level at the end of the 2004 wet season is roughly 4 m below the crest. During the remaining years, CO water levels oscillate between 70 and 84 m, never reaching the crest. ST water levels follow an analogous trend. Such sub-optimal behaviour reveals that ST is short-sighted, as it does not account for what happens beyond the 9 month horizon.

CO leads to some improvement, but it only preserves the long-term objectives to a partial extent. Alternatively, the short-sightedness may be corrected by adding a term in the RMSD objective definition to estimate future benefits/losses as function of water level and calendar month at the end of the 9 month optimization period. In case of anomalously dry conditions, the re-definition of RMSD may reduce current releases in order to increase future hydraulic heads, thus promoting a more energy-efficient useof water.

Similarly to what is seen for water levels, BS release and hydropower are oscillating significantly less than the other operation policies (Figures 10(b) and (c)). The peaks given by applying HO, LT, ST and CO are not obtained for BS. Indeed, BS water levels are generally higher than for all operation policies, thus less release is needed to produce hydropower. The abrupt changes in release and hydropower observed for CO and ST derive from the need to correct the water use according to new inflow forecasts and water level update at each monthly time-step. Release fractions (Figure 10(d)) reveal that spills occur in 2001 for HO and LT and in 2002 for LT, while CO and ST never waste water. Indeed, at the beginning of both 2001 and 2002, CO and ST water levels are significantly lowered to guarantee storage capacity for the forecasted high inflows of 2001 and 2002.

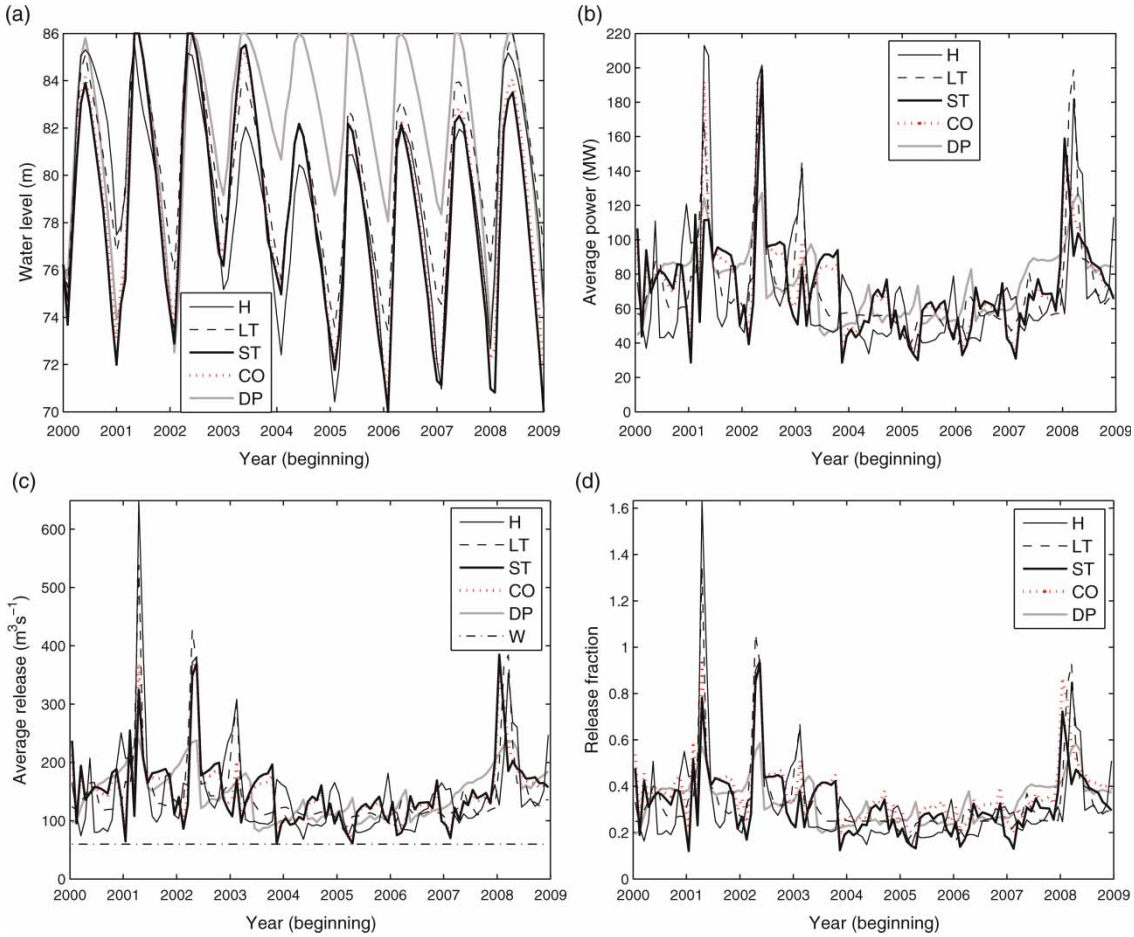

Figure 10 | Time series obtained by simulating with the 2000–2008 observed inflow: (a) reservoir water level at the beginning of each month, (b) average monthly hydropower, (c) average monthly reservoir release and (d) average monthly release fraction. HO: historical operation; LT: long-term operation optimized during 1950–1999; ST: short-term operation; CO: combined operation; BS: dynamic programming benchmark solution; and W: downstream water demand.

Discussion

The presented results show the potential improvement in reservoir management that may be achieved by coupling a GA with an effective inflow forecast technique using climatic predictions. The combined operation, acounting for short- and long-term objectives, outperforms both the historical reservoir management and the optimized traditional long-term operation using rule curves. However, the dynamic programming benchmark solution demonstrates that further improvement may be achieved. We believe that several possible directions can be investigated: (i) accounting for future benefits/losses, by adding a penalty term to RMSD, which may be a function of the reservoir state variables (water level and calendar month) at the end of the 9 month optimization period; (ii) improving the stochastic inflow forecasts by, for example, pursuing ENSO-indices that better correlate with anomalously low inflow; (iii) obtaining more detailed information about Daule Peripa, in order to formulate a more realistic reservoir simulation model; (iv) using real ENSO forecasts to account for the uncertainty of climatic forecasts in the optimization process.

CONCLUSIONS

The presented techniques showed that the management of the Daule Peripa reservoir may be improved by integrating climatic information in the reservoir operation optimization

process. The Daule Peripa reservoir, located in western Ecuador, serves a hydropower plant and a downstream water supply facility. Monthly reservoir inflow observations are available for 1950–2008, while historical releases are available only for 2000–2008. The reservoir system was simulated using time-steps not exceeding 1 month duration, during which inflow and release could be assumed constant.

Reservoir inflow is influenced by ENSO. In particular, El Niño events were found to be strongly correlated with anomalously high inflow observations. To account for such influence in the optimization, synthetic inflow time series were generated by a stochastic inflow model reproducing climate-induced inflow regime shifts and embedding ENSO-indices as covariates. SSTA measured on the Niño $1+2$ region and the Trans-Niño Index (representing the SSTA gradient over the equatorial Pacific Ocean) were used as climatic input for the stochastic inflow model. The model performed well at predicting anomalously high inflow during intense El Niño events, while anomalously low inflow was predicted less accurately. Inflow forecasts were satisfactorily performed for a lead time of 1–9 months, which is the maximum lead time of currently available ENSO forecasts.

Reservoir optimization was carried out according to the simulation-optimization approach. We used a multi-objective genetic algorithm to simultaneously minimize the root mean square hydropower deficit and the probability of not satisfying the downstream water demand. The objectives were evaluated by simulating the reservoir system using a number of synthetic inflow time series, to account for inflow uncertainty. Three reservoir operation types were defined: (i) long-term operation (LT), where rule curves guide the release as a function of water level and time of the year; (ii) short-term operation (ST), where at the beginning of each month the releases of the coming 9 months are optimized based on current inflow forecasts and water level; and (iii) combined operation (CO), in which the release is a weighted average of the optimized LT and ST releases.

The results highlight the robustness of the optimized operations. CO outperformed both historical operation and LT during 2000–2008, thus showing the potential benefit of including climatic forecasts when performing reservoir optimization. A dynamic programming benchmark solution, obtained by assuming perfect knowledge of the inflow time series, revealed that the Daule Peripa reservoir operation can be further improved. We identified two promising research directions: (i) when evaluating objectives, considering a penalty term estimating future benefits as a function of the storage at the end of the optimization period; and (ii) improving the accuracy of inflow forecasts by, for example, pursuing ENSO-indices that better correlate with anomalously low inflow.

REFERENCES

Akintuğ, B. & Rasmussen, P. F. 2005 A Markov switching model for annual hydrologic time series. *Water Resources Research* **41** (9), W09424.

Baum, L. E., Petrie, T., Soules, G. & Weiss, N. 1970 A maximization technique occurring in the statistical analysis of probabilistic functions of Markov chains. *The Annals of Mathematical Statistics* **41** (1), 164–171.

Bellman, R. 1957 *Dynamic Programming*. Princeton University Press, Princeton, NJ, USA.

Bellone, E., Hughes, J. P. & Guttorp, P. 2000 A hidden Markov model for downscaling synoptic atmospheric patterns to precipitation amounts. *Climate Research* **15** (1), 1–12.

Bertsekas, D. 2000 *Dynamic Programming and Optimal Control*. AthenaScientific, Belmont, MA, USA.

Burke, E. K. & Silva, J. D. L. 2006 The influence of the fitness evaluation method on the performance of multiobjective search algorithms. *European Journal of Operational Research* **169** (3), 875–897.

Cappè, O., Moulines, E. & Rydèn, T. (eds.). 2005 *Inference in Hidden Markov Models*. Springer Series in Statistics, New York, NY.

Chen, L. 2003 Real coded genetic algorithm optimisation of long term reservoir operation. *Journal of the American Water Resources Association* **39** (5), 1157–1165.

Deb, K., Pratap, A., Agarwal, S. & Meyarivan, T. 2002 A fast elitist non-dominated sorting genetic algorithm for multi-objective optimisation: NSGA-II. *EEE Transactions on Evolutionary Computation* **6** (2), 182–197.

Dempster, A. P., Laird, N. M. & Rubin, D. B. 1977 Maximum likelihood from incomplete data via the EM algorithm. *Journal of the Royal Statistical Society Series B-Methodological* **39** (1), 1–38.

Gelati, E., Christensen, O. B., Rasmussen, P. F. & Rosbjerg, D. 2010a Downscaling atmospheric patterns to multi-site precipitation amounts in southern Scandinavia. *Hydrology Research* **41** (3–4), 193–210.

Gelati, E., Madsen, H. & Rosbjerg, D. 2010b Markov-switching model for nonstationary runoff conditioned on El Niño information. *Water Resources Research* **46**, W02517.

Gopalakrishnan, G., Minsker, B. S. & Goldberg, D. 2001 Optimal sampling in a noisy genetic algorithm for risk-based remediation design. In: *Bridging the gap: meeting the worlds water and environmental resources challenges. Proceedings World Water and Environmental Resources Congress* (D. Phelps & G. Sehlke, eds.). ASCE, Washington DC, USA.

Hamilton, J. D. 1989 A new approach to the economic analysis of nonstationary time series and the business cycle. *Econometrica* **57** (2), 357–384.

Hughes, J. P. & Guttorp, P. 1994 A class of stochastic models for relating synoptic atmospheric patterns to regional hydrologic phenomena. *Water Resources Research* **30** (5), 1535–1546.

Hughes, J. P., Guttorp, P. & Charles, S. P. 1999 A non-homogeneous hidden Markov model for precipitation occurrence. *Journal of the Royal Statistical Society* **48** (1), 15–30.

Kapelan, Z., Savic, D. A., Walters, G. A. & Babayan, A. V. 2006 Risk- and robustness-based solutions to a multi-objective water distribution system rehabilitation problem under uncertainty. *Water Science and Technology* **53** (1), 61–75.

Kelman, J., Stedinger, J. R., Cooper, L. A., Hsu, E. & Yuan, S.-Q. 1990 Sampling stochastic dynamic programming applied to reservoir operation. *Water Resources Research* **26** (3), 447–454.

Labadie, J. W. 2004 Optimal operation of multireservoir systems: state-of-the-art review. *Journal of Water Resources Planning and Management* **130** (2), 93–111.

Loucks, D. P., Stedinger, J. R. & Haith, D. A. 1981 *Water Resource Systems Planning and Analysis*. Cornell University, Prentice-Hall Inc., Enlewood Cliffs, New Jersey, USA.

Nash, J. E. & Sutcliffe, J. V. 1970 River flow forecasting through conceptual models part I A discussion of principles. *Journal of Hydrology* **10** (3), 282–290.

Ngo, L. L., Madsen, H. & Rosbjerg, D. 2007 Simulation and optimisation modelling approach for operation of the hoa binh reservoir. *Journal of Hydrology* **336** (3–4), 269–281.

Oliveira, R. & Loucks, D. P. 1997 Operating rules for multi-reservoir systems. *Water Resources Research* **33** (4), 839–852.

Rabiner, L. R. 1989 A tutorial on hidden Markov models and selected applications in speech recognition. *Proceedings of the IEEE* **77** (2), 257–286.

Robertson, A. W., Kirshner, S. & Smyth, P. 2004 Downscaling of daily rainfall occurrence over northeast Brazil using a hidden Markov model. *Journal of Climate* **17** (22), 4407–4424.

Sharif, M. & Wardlaw, R. 2000 Multireservoir systems optimisation using genetic algorithms: case study. *Journal of Computing in Civil Engineering* **14** (4), 255–263.

Smalley, J. B. & Minsker, B. S. 2000 Risk-based in situ bioremediation design using a noisy genetic algorithm. *Water Resources Research* **36** (10), 3043–3052.

Tickle, K. S. & Goulter, I. C. 1994 Uncertainty in reservoir operation optimisation. In: *Water Policy and Management: Solving the Problems* (D. G. Fontane & H. N. Tuvel, eds.). ASCE, New York, USA, pp. 3043–3052.

Todini, E. 1999 Using phase-state modelling for inferring forecasting uncertainty in nonlinear stochastic decision schemes. *Journal of Hydroinformatics* **01.2**, 75–82.

Trenberth, K. E. 1997 The definition of El Niño. *Bulletin of the American Meteorological Society* **78** (12), 2771–2777.

Trenberth, K. E. & Stepaniak, D. P. 2001 Indices of El Niño evolution. *Journal of Climate* **14** (8), 1697–1701.

Vuille, M., Bradley, R. S. & Keimig, F. 1999 Climate variability in the Andes of Ecuador and its relation to tropical Pacific and Atlantic Sea surface temperature anomalies. *Journal of Climate* **13** (14), 2520–2535.

WCD 2000 *World Commission on Dams. Dams and Development: A New Framework for Decision-Making.* Earthscan Publications Ltd., UK.

Wu, J., Zheng, C., Chien, C. C. & Zheng, L. 2006 A comparative study of Monte Carlo simple genetic algorithm and noisy genetic algorithm for cost-effective sampling network design under uncertainty. *Advances in Water Resources* **29** (6), 899–911.

Yeh, W. 1985 Reservoir management and operations models: a state-of-the-art review. *Water Resources Research* **21** (12), 1797–1818.

First received 21 January 2010; accepted in revised form 29 September 2010. Available online June 2011

APPENDIX: THE EM ALGORITHM

At the nth iteration of the EM algorithm, the estimate of a generic parameter z is denoted $\hat{z}^{(n)}$ and the set of parameter estimates is denoted $\widehat{\boldsymbol{\theta}}^{(n)}$. Iterations are repeated until a termination criterion is satisfied. Each iteration of the EM algorithm consists of two steps. The first step (expectation) computes the conditional expected value of the log-likelihood function given the previous parameter estimates $\widehat{\boldsymbol{\theta}}^{(n-1)}$:

$$
\begin{aligned}
&E\left\{\log L(\boldsymbol{\theta}|\mathbf{a}_{1:M},\mathbf{C}_{1:M})|\widehat{\boldsymbol{\theta}}_{n-1}\right\}\\
&\quad=\sum_{i=1}^{S}\Pr\left\{s_1=i|\mathbf{a}_{1:M},\mathbf{C}_{1:M},\widehat{\boldsymbol{\theta}}^{(n-1)}\right\}\left[-\frac{1}{2}(\mathbf{c}_1-\boldsymbol{\mu}_i)'\mathbf{V}(\mathbf{c}_1-\boldsymbol{\mu}_i)\right]\\
&\qquad+\sum_{m=2}^{M}\sum_{i=1}^{S}\sum_{j=1}^{S}\Pr\left\{s_{m-1}=i,s_m=j|\mathbf{a}_{1:M},\mathbf{C}_{1:M},\widehat{\boldsymbol{\theta}}^{(n-1)}\right\}\\
&\qquad\times\left[\log p_{ij}-\frac{1}{2}(\mathbf{c}_m-\boldsymbol{\mu}_j)'\mathbf{V}(\mathbf{c}_m-\boldsymbol{\mu}_j)\right]\\
&\qquad+\sum_{m=1}^{M}\sum_{i=1}^{S}\Pr\left\{s_m=i|\mathbf{a}_{1:M},\mathbf{C}_{1:M},\widehat{\boldsymbol{\theta}}^{(n-1)}\right\}\\
&\qquad\times\left[\log\frac{1}{\sigma_i\sqrt{2\pi}}-\frac{(a_m-\delta_i-a_{m-1}\lambda_i-\mathbf{c}'_m\gamma_i)^2}{2\sigma_i^2}\right]
\end{aligned}
\tag{A 1}
$$

where $\mathbf{a}_{1:M}$ and $\mathbf{C}_{1:M}$ are the time series of a_m and $\mathbf{c}_m$, respectively, from month 1 to M, which is the last monthly time-step.

The second step (maximization) maximizes Equation (A 1) with respect to the model parameters and obtains the new estimates $\widehat{\boldsymbol{\theta}}^{(n)}$. To perform such maximization we need to compute the conditional state probability terms with the Baum–Welch algorithm (Baum *et al.* 1970; Rabiner 1989). A description of the Baum–Welch algorithm for non-homogeneous hidden Markov models is available in Gelati *et al.* (2010a), and is applicable to the presented Markov-switching model after minor modifications.

To obtain $\widehat{p}_{ij}^{(n)}$, we maximize Equation (A 1) using Lagrange multipliers to enforce the constraints $\sum_{j=1}^{S}p_{ij}=1$ (for $i=1,\ldots,S$). We therefore define the function:

$$
\begin{aligned}
w_p(p_{ij},\psi)&=\sum_{m=2}^{M}\Pr\left\{s_{m-1}=i,s_m=j|\mathbf{a}_{1:M},\mathbf{C}_{1:M},\widehat{\boldsymbol{\theta}}^{(n-1)}\right\}\\
&\quad\times\log p_{ij}+\psi\left(1-\sum_{j=1}^{S}p_{ij}\right)
\end{aligned}
\tag{A 2}
$$

which collects the terms of Equation (A 1) that do not reduce to zero when computing the derivative in p_{ij}. Imposing $(\partial w_p/\partial p_{ij})=0$, we obtain:

$$
\sum_{m=2}^{M}\Pr\frac{\left\{s_{m-1}=i,s_m=j|\mathbf{a}_{1:M},\mathbf{C}_{1:M},\widehat{\boldsymbol{\theta}}^{(n-1)}\right\}}{p_{ij}}-\psi=0 \tag{A 3}
$$

Applying the constraint $\sum_{j=1}^{S}p_{ij}=1$, we find that

$$
\begin{aligned}
\psi&=\sum_{j=1}^{S}\Pr\left\{s_{m-1}=i,s_m=j|\mathbf{a}_{1:M},\mathbf{C}_{1:M},\widehat{\boldsymbol{\theta}}^{(n-1)}\right\}\\
&=\Pr\left\{s_{m-1}=i|\mathbf{a}_{1:M},\mathbf{C}_{1:M},\widehat{\boldsymbol{\theta}}^{(n-1)}\right\}
\end{aligned}
\tag{A 4}
$$

Thus, the estimate of p_{ij} is:

$$
\widehat{p}_{ij}^{(n)}=\frac{\sum_{m=2}^{M}\Pr\left\{s_{m-1}=i,s_m=j|\mathbf{A}_{1:M},\mathbf{C}_{1:M},\widehat{\boldsymbol{\theta}}^{(n-1)}\right\}}{\sum_{m=2}^{M}\Pr\left\{s_{m-1}=i|\mathbf{A}_{1:M},\mathbf{C}_{1:M},\widehat{\boldsymbol{\theta}}^{(n-1)}\right\}} \tag{A 5}
$$

To compute $\widehat{\boldsymbol{\mu}}_j^{(n)}$, we define the function:

$$
\begin{aligned}
w_\mu(\boldsymbol{\mu}_j)&=\Pr\left\{s_1=j|\mathbf{a}_{1:M},\mathbf{C}_{1:M},\widehat{\boldsymbol{\theta}}^{(n-1)}\right\}\\
&\quad\times\left[-\frac{1}{2}(\mathbf{c}_1-\boldsymbol{\mu}_j)'\mathbf{V}(\mathbf{c}_1-\boldsymbol{\mu}_j)\right]\\
&\quad+\sum_{m=2}^{M}\sum_{i=1}^{S}\Pr\left\{s_{m-1}=i,s_m=j|\mathbf{a}_{1:M},\mathbf{C}_{1:M},\widehat{\boldsymbol{\theta}}^{(n-1)}\right\}\\
&\quad\times\left[-\frac{1}{2}(\mathbf{c}_m-\boldsymbol{\mu}_j)'\mathbf{V}(\mathbf{c}_m-\boldsymbol{\mu}_j)\right]\\
&=\sum_{m=1}^{M}\Pr\left\{s_m=j|\mathbf{a}_{1:M},\mathbf{C}_{1:M},\widehat{\boldsymbol{\theta}}^{(n-1)}\right\}\\
&\quad\times\left[-\frac{1}{2}(\mathbf{c}_m-\boldsymbol{\mu}_j)'\mathbf{V}(\mathbf{c}_m-\boldsymbol{\mu}_j)\right]
\end{aligned}
\tag{A 6}
$$

which collects the terms of Equation (A 1) that do not reduce to zero when computing the gradient in $\boldsymbol{\mu}_j$. Imposing $\nabla_{\mu_j} w_\mu = 0$ (where 0 is a N-long zero vector and where N is the length of $\mathbf{c}_m$):

$$\sum_{m=1}^{M} \Pr\left\{s_m = j | \mathbf{a}_{1:M}, \mathbf{C}_{1:M}, \widehat{\boldsymbol{\theta}}^{(n-1)}\right\}(\mathbf{c}_m - \boldsymbol{\mu}_j) = 0 \tag{A 7}$$

Thus, the estimate of $\boldsymbol{\mu}_j$ is:

$$\widehat{\boldsymbol{\mu}}_j^{(n)} = \frac{\sum_{m=2}^{M} \Pr\left\{s_m = j | \mathbf{a}_{1:M}, \mathbf{C}_{1:M}, \widehat{\boldsymbol{\theta}}^{(n-1)}\right\}\mathbf{c}_m}{\sum_{m=1}^{M} \Pr\left\{s_m = j | \mathbf{a}_{1:M}, \mathbf{C}_{1:M}, \widehat{\boldsymbol{\theta}}^{(n-1)}\right\}} \tag{A 8}$$

To obtain the estimates of the ARX spill parameters (δ_i, λ_i, γ_i and σ_i), we define the function:

$$\begin{aligned} w_{ARX}(\delta_1, \ldots, \delta_S, \lambda_1, \ldots, \lambda_S, \gamma_1, \ldots, \gamma_S, \sigma_1, \ldots, \sigma_S) \\ = \sum_{m=1}^{M}\sum_{i=1}^{S} \Pr\left\{s_m = i | \mathbf{a}_{1:M}, \mathbf{C}_{1:M}, \widehat{\boldsymbol{\theta}}^{(n-1)}\right\} \\ \times \left[\log \frac{1}{\sigma_i\sqrt{2\pi}} - \frac{(a_m - \delta_i - a_{m-1}\lambda_i - \mathbf{c}'_m\boldsymbol{\gamma}_i)^2}{2\sigma_i^2}\right] \end{aligned} \tag{A 9}$$

Imposing $(\partial w_{ARX}/\partial \delta_i) = 0$, $(\partial w_{ARX}/\partial \lambda_i) = 0$, $\nabla_{\gamma_i} w_{ARX} = 0$, and $(\partial w_{ARX}/\partial \sigma_i) = 0$, we obtain:

$$\sum_{m=1}^{M} \Pr\left\{s_m = i | \mathbf{a}_{1:M}, \mathbf{C}_{1:M}, \widehat{\boldsymbol{\theta}}^{(n-1)}\right\} \times (a_m - \delta_i - \lambda_i a_{m-1} - \mathbf{c}'_m\boldsymbol{\gamma}_i) = 0 \tag{A 10}$$

$$\sum_{m=1}^{M} \Pr\left\{s_m = i | \mathbf{a}_{1:M}, \mathbf{C}_{1:M}, \widehat{\boldsymbol{\theta}}^{(n-1)}\right\} \times (a_m - \delta_i - \lambda_i a_{m-1} - \mathbf{c}'_m\boldsymbol{\gamma}_i)a_{m-1} = 0 \tag{A 11}$$

$$\sum_{m=1}^{M} \Pr\left\{s_m = i | \mathbf{a}_{1:M}, \mathbf{C}_{1:M}, \widehat{\boldsymbol{\theta}}^{(n-1)}\right\} \times \mathbf{c}_m(a_m - \delta_i - \lambda_i a_{m-1} - \mathbf{c}'_m\boldsymbol{\gamma}_i) = 0 \tag{A 12}$$

$$\sum_{m=1}^{M} \Pr\left\{s_m = i | \mathbf{a}_{1:M}, \mathbf{C}_{1:M}, \widehat{\boldsymbol{\theta}}^{(n-1)}\right\} \times [(a_m - \delta_i - a_{m-1}\lambda_i - \mathbf{c}'_m\boldsymbol{\gamma}_i)^2 - \sigma_i^2] = 0 \tag{A 13}$$

Equations (A 10), (A 11) and (A 12) constitute a linear system of $2 + N$ equations in $2 + N$ unknown variables (δ_i, λ_i and the components of $\boldsymbol{\gamma}_i$):

$$\mathbf{X}_i \begin{bmatrix} \delta_i \\ \lambda_i \\ \boldsymbol{\gamma}_i \end{bmatrix} = \mathbf{b}_i \tag{A 14}$$

where

$$\begin{aligned} \mathbf{X}_i = \sum_{m=1}^{M} \Pr\left\{s_m = i | \mathbf{a}_{1:M}, \mathbf{C}_{1:M}, \widehat{\boldsymbol{\theta}}^{(n-1)}\right\} \\ \times \begin{bmatrix} 1 & a_{m-1} & \mathbf{c}'_m \\ a_{m-1} & a_{m-1}^2 & a_{m-1}\mathbf{c}'_m \\ \mathbf{c}_m & a_{m-1}\mathbf{c}_m & \mathbf{c}_m\mathbf{c}'_m \end{bmatrix} \end{aligned} \tag{A 15}$$

and

$$\begin{aligned} \mathbf{b}_i = \sum_{m=1}^{M} \Pr\left\{s_m = i | \mathbf{a}_{1:M}, \mathbf{C}_{1:M}, \widehat{\boldsymbol{\theta}}^{(n-1)}\right\} \\ \times \begin{bmatrix} a_m \\ a_{m-1}a_m \\ a_m\mathbf{c}_m \end{bmatrix} \end{aligned} \tag{A 16}$$

The estimates of δ_i, λ_i and γ_i are obtained by solving Equation (A14):

$$\begin{bmatrix} \widehat{\delta}_i^{(n)} \\ \widehat{\lambda}_i^{(n)} \\ \widehat{\boldsymbol{\gamma}}_i^{(n)} \end{bmatrix} = \mathbf{X}_i^{-1}\mathbf{b}_i \tag{A 15}$$

The estimate of σ_i is computed by substituting the estimates obtained from Equation (A 15) into Equation (A 13):

$$\widehat{\sigma}_i^{(n)} = \sqrt{\frac{\sum_{m=1}^{M} \Pr\left\{s_m = i \middle| \mathbf{a}_{1:M}, \mathbf{C}_{1:M}, \widehat{\boldsymbol{\theta}}^{(n-1)}\right\} \times \left(a_m - \widehat{\delta}_i^{(n)} - a_{m-1}\widehat{\lambda}_i^{(n)} - \mathbf{c}'_m\widehat{\boldsymbol{\gamma}}_i^{(n)}\right)^2}{\sum_{m=1}^{M} \Pr\left\{s_m = i \mathbf{a}_{1:M}, \mathbf{C}_{1:M}, \widehat{\boldsymbol{\theta}}^{(n-1)}\right\}}} \tag{A 16}$$